Eur. Phys. J. B **41**, 207–212 (2004)
DOI: 10.1140/epjb/e2004-00311-x

THE EUROPEAN PHYSICAL JOURNAL B

Pair correlations and interaction energies in FePd single crystal

T. Mehaddene[1,a], J.M. Sanchez[2], R. Caudron[3], M. Zemirli[4], and V. Pierron-Bohnes[5]

[1] Physik Department E13/FRM II, TU München, James-Franck Str. 1, 85747 Garching, Germany
[2] Texas Materials Institute, University of Texas, Austin, Texas 78712, USA
[3] LEM (ONERA-CNRS), 29 avenue de la division Leclerc, BP 72, 92320 Châtillon/Bagneux and Léon Brillouin Laboratory (CEA-CNRS), CEA-Saclay, 91190 Gif-sur-Yvette, France
[4] LPCQ, Université Mouloud Mammeri, 15000 Tizi-Ouzou, Algeria
[5] IPCMS, CNRS-ULP, 23 rue du Loess, BP 43, 67034 Strasbourg Cedex 2, France

Received 15 April 2004 / Received in final form 11 August 2004
Published online 12 October 2004 –

Abstract. Diffuse neutron scattering measurements were carried out in a FePd single crystal at 1020 K in the (100) and (110) reciprocal planes. The diffuse intensity is nearly symmetric, showing that the static displacements are small. A set of displacement and short-range order parameters have been fitted to the measured data using a least square procedure. The short-range order parameters have been used in conjunction with an inverse cluster variation method to deduce the pair interaction energies. A strong attractive interaction between second nearest-neighbour like atoms is found.

PACS. 61.12.Ex Neutron scattering – 64.60.Cn Order-disorder transformations – 61.66.Dk Alloys

1 Introduction

In solid solutions, chemical short-range order (SRO) is a direct manifestation of effective interaction energies that, in many instances, determine the thermodynamic behavior of the system. Thus, measurements of diffuse scattering aimed at characterizing chemical SRO have been the subject of numerous studies and reports in the scientific literature [1–13]. The primary motivation of such studies is to gain understanding of the local atomic arrangements and their role on the magnetic, mechanical and thermodynamic properties of the alloy.

Measurement of diffuse scattering is the method of choice to determine the local atomic arrangement in alloys. Over the last 50 years, experimental techniques for diffuse scattering measurements have evolved significantly and, at present, they are carried out with a high degree of accuracy in single crystals at high and low temperature [1–13]. The methodology to determine the Warren-Cowley SRO parameters from the experimental diffuse intensity is also well established and routinely used to calculate the pair correlation functions and effective pair interactions. Specifically, the theoretical description of the pair correlations is carried out using standard statistical methods, such as cluster variation method (CVM) [14–16] or Monte Carlo simulations [17], and typically rely on model Hamiltonians that include interaction energies for a large set of clusters [18]. It should be noted that the analysis of the diffuse scattering by the CVM, although computationally more demanding, offers a significant improvement over the use of the Bragg-Williams approximation [19], as pioneered by Cowley [20], Krivoglaz [21], and Clapp and Moss [22].

The most commonly used approach to compute the effective pair interactions is the real-space inverse CVM introduced by Gratias and Cénédèse [23]. In this method, the effective pair interactions are obtained by fitting the Warren-Cowley SRO parameters in real space which, in turn, are related by a Fourier transform to the experimentally determined SRO intensity.

While the inverse CVM method is relatively straightforward to implement, it becomes computationally very intensive for large cluster approximations. Thus, the fitting is typically done for a relatively small number of SRO parameters which, in turn, results in interactions that may be unrealistically short-range for the alloy under investigation. As described in Section 4, this computational limitation of the inverse CVM method can be effectively overcome by using a CVM approximation that combines a set of computationally manageable compact clusters plus pairs (i.e. two-point clusters) that extend to the desired interaction range. An alternative approach that has been used consists in fitting the pair correlations by an inverse Monte Carlo method in real space, in which case longer interaction ranges may be included without any significant computational overhead [5,10].

In this paper, we describe high-temperature neutron diffuse scattering measurements in FePd. Around

[a] e-mail: mtarik@ph.tum.de

the 50/50 stoichiometry, FePd orders in the $L1_0$ structure, made of alternating pure iron and pure palladium (001) planes [24]. This very anisotropic chemical order is accompanied by a strong magnetic anisotropy and a tetragonality $c/a \approx 0.97$. The pronounced anisotropic properties of FePd are at the core of the present renewed interest in this system. In thin films, $L1_0$ FePd alloys display, in addition to a high magnetic anisotropy, a magnetization that is perpendicular to the film surface [25,26], thus making such films good candidates for magneto-optical-storage devices. Furthermore, the combination of the cubic to tetragonal symmetry change at the order-disorder transition and the rapid ordering kinetics of this phase transformation make FePd alloys high temperature shape memory materials [27] with potential applications as actuators and coupling devices. Consequently, an additional motivation of the current study was to provide a detailed characterization of the chemical order and of the underlying interaction energies in a system with potentially important engineering applications.

This paper is organised as follows: we present a summary of the experimental procedure together with the method used to obtain the elastic diffuse intensity (deconvolution process and corrections) in Section 2. In Section 3, a set of Warren-Cowley SRO parameters is obtained from the corrected data. These SRO parameters are used in Section 4 to calculate the pair interaction energies using an inverse CVM method. Concluding remarks are given in Section 5.

2 Diffuse neutron scattering

The measurements of diffuse scattering were carried out within the face centered cubic (fcc) temperature range of FePd. To avoid the critical effects near to the order-disorder temperature ($T_c = 920$ K), we performed the measurements at 1020 K using a parallelepiped single crystal, lent to us by Professor Tanaka (Kyoto, Japan) [27]; the same sample was previously used to measure the normal modes of vibration by inelastic neutron scattering [28].

We carried out the measurements on the G4-4 two-axis spectrometer in Léon Brillouin Laboratory (CEA-CNRS, Saclay, France) with the wavelength $\lambda = 0.28$ nm. A high temperature furnace is located at the center of a 80 cm diameter vacuum vessel (vacuum better than 10^{-5} torr). The detection device is a bank of 64 He^3 detectors: 48 large detectors (50 mm in diameter) placed every 2.5° and 16 smaller detectors (10 mm in diameter) placed every 0.625° at small angles. The accessible diffraction vectors range is between 0.2 and 2.8 reciprocal lattice units (RLU)(1RLU=$2\pi/a$ with $a = 0.388$ nm for the fcc FePd). The (100) and (110) planes are scanned by a rotation of the sample with a step $\Delta\omega = 4°$. This leads to a sampling mesh of about 3000 measurement points on the two scattering planes.

At high temperature, an energy analysis is necessary to extract the elastic contribution out of the measured intensity. It was performed using a time-of-flight setup. The elastic contribution was obtained by the deconvolution of the time-of-flight spectra and the impulse response of the spectrometer [29]. Due to the long wavelength used, the dominant inelastic process is the phonon annihilation located on the high-energy side of the spectrum, except in the close vicinity of the Bragg peaks where many points had to be eliminated due to a strong quasi-elastic scattering which arises mainly from the annihilation of low-frequency acoustical phonons.

Standard corrections were applied to the data. The absorption coefficients [30] and multiple scattering corrections [31] were evaluated using a Monte Carlo integration method. The dynamic Debye-Waller factor was calculated from the inelastic neutron scattering results [28] using the Krivoglaz method [21]. The possible deviation of the total Debye-Waller factor, due to static contribution and quasi-harmonic deviations [32], were adjusted from the data. The instrumental background has been measured with the empty furnace. We eliminated all the points where the furnace signal is large (powder rings of the resistor) inducing a large error bar (white circles in Figs. 1). In order to calibrate the efficiency of the detectors, we measured at room temperature a vanadium probe with the same shape, dimensions, and position in the furnace as the sample. The data were finally normalised to the number of atoms in the beam. Due to the low contrast between the scattering lengths of Fe and Pd ($\Delta b = 3.54$ fm), the whole measurements lasted four weeks to get a good signal/noise ratio.

3 Short-range order parameters

Figure 1 displays the corrected intensities in the two reciprocal planes. The diffuse intensity is mainly located around 100 and equivalent points. The static displacements give rise to a weak asymmetry of the diffuse peaks. An increase in the diffuse intensity can be observed close to the origin, due to the paramagnetic contribution of the Fe atom moments. The corresponding points have been eliminated in the SRO analysis.

The corrected intensity at the reciprocal space point $\mathbf{k} = \frac{2\pi}{a}(h_1, h_2, h_3)$ is given by:

$$I_{corr}(\mathbf{k}) = \alpha(\mathbf{k}) + \sum_{i=1}^{3} h_i Q_i(\mathbf{k}) + I_{inc}. \qquad (1)$$

$\alpha(\mathbf{k})$ is the SRO contribution. The $Q_i(\mathbf{k})$'s are related to the Fourier transform of the static atomic displacements. I_{inc} is the incoherent scattering cross section per atom in Laue units (1LU= $\pi(b_{\mathrm{Fe}} - b_{\mathrm{Pd}})^2 = 39.6 \times 10^{-30}$ m^2, with b_{Fe} and b_{Pd} the coherent scattering lengths for Fe and Pd, respectively): $I_{inc} = 0.632$LU in FePd. Equation (1) is the development up to the first order in the displacement $\mathbf{u}_p$ at lattice site $\mathbf{R_p} = \frac{a}{2}(l, m, n)$, where $\mathbf{p}$ stands for the integers (l, m, n), also noted (lmn). The SRO contribution to the diffuse intensity is given by the Fourier transform of the Warren-Cowley SRO parameters $\alpha_{\mathbf{p}}$ [20]:

$$\alpha(\mathbf{k}) = \sum_{\mathbf{p}} \alpha_{\mathbf{p}} \cos(\mathbf{k} \cdot \mathbf{R_p}) \qquad (2)$$

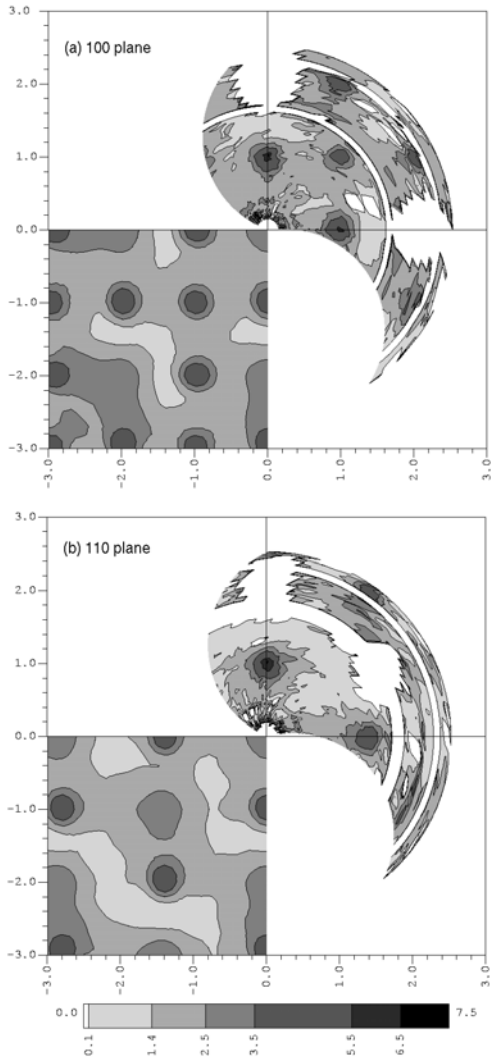

Fig. 1. Corrected experimental intensities and reconstructed intensities (down left) in the (100) (a) and (110) (b) reciprocal planes. The typical error bar is about 0.4LU.

The Warren-Cowley SRO parameters are related to the correlation functions by:

$$\alpha_{\mathbf{p}} = \frac{\langle \sigma_{\mathbf{0}} \sigma_{\mathbf{p}} \rangle - \langle \sigma_{\mathbf{0}}^2 \rangle}{1 - \langle \sigma_{\mathbf{0}} \rangle^2} \tag{3}$$

where $\sigma_{\mathbf{0}}$ and $\sigma_{\mathbf{p}}$ are the occupation operators at the origin and site $\mathbf{p}$, respectively. These occupation operators are equal to 1 or -1 when the lattice site is occupied by Fe or Pd atoms, respectively. The brackets stand for configurational averages.

In equation (2), α_0 is theoretically equal to 1. Due to the uncertainty in the measured diffuse intensity near the Bragg peaks, we have fixed this value assuming: $\alpha(\mathbf{0}) = 1$. The sensitivity of the results to this assumption is very small.

The quantities $\mathbf{Q} = [Q_1, Q_2, Q_3]$ in equation (1) are given by:

$$\mathbf{Q}(\mathbf{k}) = \sum_{\mathbf{p}} \gamma_{\mathbf{p}} \sin(\mathbf{k} \cdot \mathbf{R}_{\mathbf{p}}). \tag{4}$$

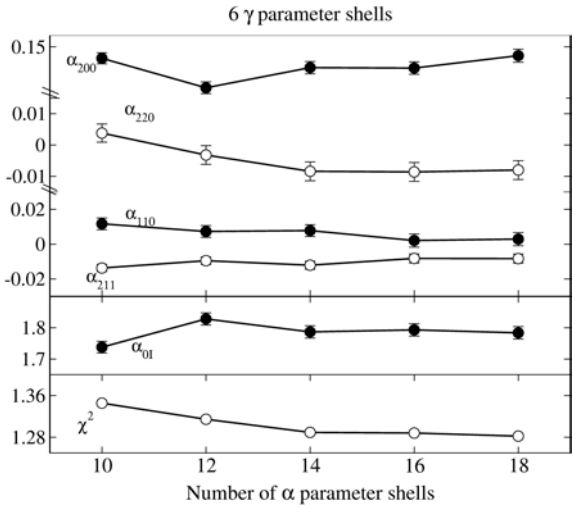

Fig. 2. Sensitivity of the first four SRO parameters, the constant contribution $\alpha_{0I} = \alpha_0 + I_{inc}$ and the squared residual error χ^2 to the number of the SRO parameter in the fit.

The first-order displacement parameters $\gamma_{\mathbf{p}}$ are defined by

$$\gamma_{\mathbf{p}} = -\frac{2\pi}{a} \sum_{i,j} \frac{b_i b_j}{F_{Laue}} \rho_{2,\mathbf{p}}(ij) \langle \Delta \mathbf{u_p}^{ij} \rangle. \tag{5}$$

$\langle \Delta \mathbf{u_p}^{ij} \rangle$ is the average relative displacement between atoms of type i and j (i.e. Fe or Pd) separated by $\mathbf{R_p}$. $\rho_{2,\mathbf{p}}(ij)$ is the probability of finding atoms i and j at a distance $\mathbf{R_p}$, equal to $(1+\alpha_{\mathbf{p}})/4$ and $(1-\alpha_{\mathbf{p}})/4$ for like atom (FeFe or PdPd) and un-like atom (FePd) pairs respectively. F_{Laue} is the usual normalization factor: $F_{Laue} = (b_{\mathrm{Fe}} - b_{\mathrm{Pd}})^2/4$ in equiatomic FePd.

We have adjusted the Warren-Cowley SRO parameters fitting the corrected data by a least square procedure with a weight inversely proportional to the squared experimental error ΔI^2. We have minimized the squared residual error:

$$\chi^2 = \sum \frac{(I_m - I_c)^2}{N_{free} \Delta I^2}. \tag{6}$$

I_m and I_c are the measured and calculated intensities respectively. $N_{free} = N_{points} - N_{variables}$ is the number of degrees of freedom of the fit. N_{points} and $N_{variables}$ are the number of experimental points and of variables in the fit.

We have verified the stability of the fit by varying the number of shells for the SRO parameters up to 18, and those for the displacements up to 16. The sensitivity of the results to the number of SRO parameters is shown in Figure 2 for the four first SRO parameters. Above 14 SRO parameters and 6 displacement parameters, the residual error does not vary significantly and all calculated intensities are stable. In the following, we discuss the results obtained with 14 shells for the SRO parameters and 6 shells for the displacement parameters. The constant contribution to the cross section, α_{0I}, is the sum of the $\alpha_0 = 1$ term and the sample incoherent contribution. Its expected value is thus 1.63(18)LU. We obtained 1.76(2)LU, which is slightly smaller than the expected value but remains within the error bar.

Table 1. Displacement parameters deduced from the adjustment of the experimental data.

i	lmn	γ_{ix}	$\Delta\gamma_{ix}$	γ_{iy}	$\Delta\gamma_{iy}$	γ_{iz}	$\Delta\gamma_{iz}$
1	110	–0.0459	0.0023	–0.0459	0.0023		
2	200	0.0449	0.0058				
3	211	–0.0007	0.0018	–0.0063	0.0013	–0.0063	0.0013
4	220	0.0059	0.0027	0.0059	0.0027		
5	310	0.0021	0.0020	0.0042	0.0022		
6	222	–0.0057	0.0020	–0.0057	0.0020	–0.0057	0.0020

Table 2. Warren-Cowley SRO parameters and the deduced pair interaction energies (in meV) with the corresponding error bars.

shell (i)	lmn	$2R_{lmn}/a$	α_{lmn}	$\Delta\alpha_{lmn}$	V_{lmn}	ΔV_{lmn}
1	110	1.141	0.0019	0.0037	–0.43	0.33
2	200	2.000	0.1399	0.0056	–11.76	1.11
3	211	2.449	–0.0079	0.0022	0.47	0.20
4	220	2.828	0.0379	0.0030	0.85	0.88
5	310	3.162	–0.0225	0.0023	1.97	0.20
6	222	3.464	0.0295	0.0030	–1.54	0.63
7	321	3.741	–0.0127	0.0016	1.11	0.14
8	400	4.000	0.0244	0.0045	–2.14	0.40
9	330	4.242	–0.0030	0.0027	0.26	0.23
10	411	4.242	–0.0135	0.0019	1.18	0.16
11	420	4.472	0.0135	0.0022	–1.18	0.19
12	332	4.690	–0.0081	0.0019	0.71	0.16
13	422	4.898	0.0138	0.0018	–1.21	0.16
14	431	5.099	–0.0096	0.0013	0.84	0.11

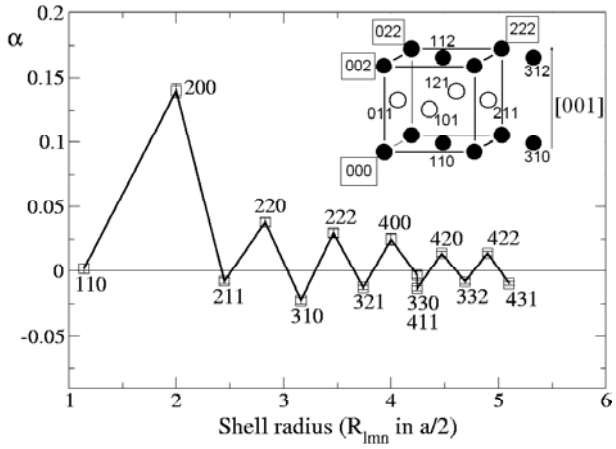

Fig. 3. Variation of the Warren-Cowley SRO parameters with the distance in FePd at 1020K. The labels give the atom positions in a/2 units. In insert: the $L1_0$ ordered phase with the different atomic occupations (•: Fe and o: Pd). The positions always occupied by Fe are framed.

The values of $\gamma_{\mathbf{p}}$ and $\alpha_{\mathbf{p}}$ are given in Tables 1 and 2 respectively. The $\alpha_{\mathbf{p}}$ are plotted in Figure 3. The largest SRO parameter is α_{200}, showing a strong attraction between second nearest-neighbour like atoms. The signs of the SRO parameters can be related to the nature of pairs in the $L1_0$ ordered structure. Neglecting the small tetragonality of the $L1_0$ structure and indexing the points in the fcc lattice, we get clearly positive values for like atom pairs in $L1_0$ ($\alpha_{l,m,n}$ with l, m and n all even) and small values for pairs that are mixed (like and un-like atoms) in $L1_0$ ($\alpha_{l,m,n}$ with two odds and one even number among l, m and n), as shown in the insert of Figure 3.

Figure 1 compares the diffuse intensities, reconstructed using equation (1), to the experimental intensities. The results of the adjustment are in good agreement with the experimental data. The diffuse intensity is nearly symmetrical (small displacement contribution) in spite of the large size difference between Fe and Pd atoms. The diffuse intensity is mostly concentrated near 100 and equivalent points, i.e. the positions of the superstructure peaks in the long-range ordered $L1_0$ structure. It is not always the case: in the Pt-V and Ni-V systems the SRO diffuse intensity above T_c and the long-range order peaks below T_c are differently located [4,9].

4 Effective pair interaction energies

Using the Generalised Perturbation Method, Gautier, Ducastelle and co-workers [33,34] have shown that the total energy of the alloy formation can be written as the sum of a non-local energy term, associated with the random alloy, plus a local ordering contribution that can be approximated as a sum of concentration dependent many-body contributions. Bieber and Gautier [35] have shown that in the transition metal alloys the predominant terms of the latter expansion are the pair interaction terms.

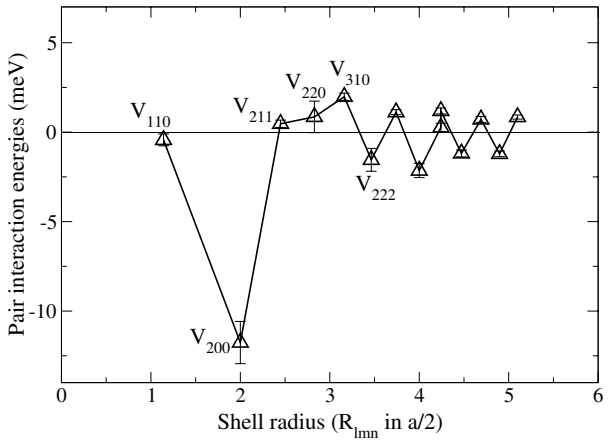

Fig. 4. Pair interaction energies in FePd at 1020 K. The labels give the atom positions in a/2 units.

In order to extract the pair interactions from the experimental values of the Warren-Cowley SRO parameters, we consider an Ising Hamiltonian which contains effective pair interactions:

$$H = \frac{1}{2} \sum_{\mathbf{p},\mathbf{p}'} V^c_{\mathbf{p},\mathbf{p}'} \sigma_{\mathbf{p}} \sigma_{\mathbf{p}'}, \qquad (7)$$

where $\sigma_{\mathbf{p}}$ is the occupation operator on the site $\mathbf{R_p}$ defined in equation (3) and $V^c_{\mathbf{p},\mathbf{p}'}$ is the effective chemical interaction between atoms at sites $\mathbf{R_p}$ and $\mathbf{R_{p'}}$.

In the Fe–Al system, that is magnetically very similar to the Fe–Pd system, some of us have shown [1,2] that the interplay between chemical and magnetic SRO is negligible above $T/T_{Curie} = 1.2$. In FePd, $T_{Curie} =$ 760 K. The measurement temperature is thus high enough ($T/T_{Curie} = 1.34$) to neglect the magnetic SRO.

We have calculated the effective pair interaction energies from the Warren-Cowley SRO parameters using the inverse CVM method proposed by Gratias and Cénédèse [23]. The method consists in minimizing a free energy functional where the entropy is a linear combination of entropies of finite clusters included in a given basic cluster. According to an optimized procedure for selecting the basic cluster [36], a very accurate approximation for the fcc lattice consists in using two maximum clusters, the face centered cube and the 13-points cubo-octahedron [37]. However, this cluster combination allows the calculation of only the first four and the sixth effective pair interactions. Therefore we have used a CVM approximation that includes, in addition to the face centered cube and the 13-points cubo-octahedron clusters, fifth neighbour pair and all other pairs from the 7th up to the 14th neighbours.

The calculated pair interactions are given in Table 2 and plotted in Figure 4. We note that despite the high value of the transition temperature (920 K), the first pair interaction energy is almost zero. The stability of the $L1_0$ structure is mainly due to the predominant second pair interaction and the oscillatory behavior of the V_{lmn}: when only like atom pairs are present in the $L1_0$ phase, $V_{lmn} < 0$, whereas when both like and un-like atom pairs are present in the $L1_0$ phase, $V_{lmn} > 0$. The predominance of the second pair interaction has been also recently observed in Fe–Pt system [38].

The pair interaction energies have been used to calculate the order-disorder transition temperature in FePd by a Monte-Carlo simulation of the disordering process of the ordered state. The model used has been described in details in previous papers [39–41] and the detailed results will be published in a forthcoming paper [42]. The obtained order-disorder transition temperature compares well with the expected value.

5 Conclusion

Atomic pair correlation functions have been measured in a FePd single crystal by diffuse neutron scattering and have been used to deduce the pair interaction energies. In spite of the atomic size difference between Fe and Pd and the tetragonality of the $L1_0$ ordered structure, the local lattice distortions are small. The diffuse intensity is nearly symmetric and shows the signature of a highly stable $L1_0$ phase mainly due to predominant second pair interaction energy V_{200} and alternating behavior of V_{lmn} for shells containing like atom (l, m and n all even) and un-like atom pairs (2 odds and one even number among l, m and n) in the $L1_0$ ordered structure.

Finally, we point out that our results show the effective pair interaction range in FePd extending over many atomic shells and, thus, we offer a word of caution regarding the adequacy of previous descriptions of the Fe-Pd system using only nearest-neighbour pair interaction [43].

We would like to thank Pr. Tanaka and Pr. Numakura who provided us with the single crystal. This work was partly supported by Algerian project ANDRU/PNR3 (AU49902) and by a collaborative program 99 MDU 449 between the University Louis Pasteur of Strasbourg, France and the University Mouloud Mammeri of Tizi-Ouzou, Algeria.

References

1. V. Pierron-Bohnes, S. Lefebvre, M. Bessière, A. Finel, Acta Metall. Mater. **34**, 2701 (1990)
2. V. Pierron-Bohnes, M.C. Cadeville, A. Finel, O. Schaerpf, J. Phys. I France **1**, 1247 (1991)
3. V. Pierron-Bohnes, E. Kentzinger, M.C. Cadeville, J.M. Sanchez, R. Caudron, F. Solal, R. Kozubski, Phys. Rev. B **51**, 5760 (1995)
4. F. Solal, R. Caudron, F. Ducastelle, A. Finel, A. Loiseau, Phys. Rev. Lett. **58**, 2245 (1987)
5. W. Schweika, H.-G. Haubold, Phys. Rev. B **37**, 9240 (1988)
6. B. Schönfeld, L. Reinhard, G. Kostorz, W. Bührer, Acta Mater. **45**, 5187 (1997)
7. M. Capitan, S. Lefebvre, Y. Calvayrac, M. Bessière, P. Cénédèse, J. Appl. Crystallogr. **32**, 1039 (1999)
8. E. Kentzinger, V. Parasote, V. Pierron-Bohnes, J.F. Lami, M.C. Cadeville, Phys. Rev. B **61**, 14975 (2000)

9. D. Le Bolloc'h, A. Finel, R. Caudron, Phys. Rev. B **62**, 12082 (2000)
10. M.J. Portmann, B. Schönfeld, G. Kostorz, F. Altorfer, Phys. Rev. B **65**, 24110 (2001)
11. D. Le Bolloc'h, J.L. Robertson, H. Reichert, S.C. Moss, M.L. Crow, Phys. Rev. B **63**, 35204 (2001)
12. M. Prem, G. Krexner, F. Pettinari-Sturmel, N. Clement, Appl. Phys. A **74**, S1112 (2002)
13. K. Osaka, T. Takama, Acta Mater. **50**, 1289 (2002)
14. R. Kikuchi, Phys. Rev. **81**, 988 (1951)
15. J.M. Sanchez, Physica A **111**, 200 (1982)
16. T. Mohri, J.M. Sanchez, D. de Fontaine, Acta Metall. **33**, 1463 (1985)
17. V. Gerold, J. Kern, Acta Metall. **35**, 393 (1987)
18. J.M. Sanchez, F. Ducastelle, D. Gratias, Physica A **128**, 334 (1984)
19. W.L. Bragg, E.J. Williams, Proc. R. Soc. London Ser. A **145**, 69 (1934)
20. J.M. Cowley, J. Appl. Phys. **21**, 24 (1950)
21. M.A. Krivoglaz, *Theory of X-ray and thermal neutron scattering by real crystals* (Plenum Press, 1966)
22. P.C. Clapp, S.C. Moss, Phys. Rev. **142**, 418 (1966)
23. D. Gratias, P. Cénédèse, J. Phys. Colloq. France **46**, C9-149 (1985)
24. O. Kubachewski, *Iron Binary Phase Diagrams* (Springer Verlag N.Y., 1982)
25. V. Gehanno, A. Marty, B. Gilles, Y. Samson, Phys. Rev. B **55**, 12552 (1997)
26. P. Kamp, A. Marty, B. Gilles, R. Hoffmann, M. Marchesini, M. Belakhovsky, C. Boeglin, H.A. Dürr, S.S. Dhesi, G. van der Laan, A. Rogalev, Phys. Rev. B **59**, 1105 (1999)
27. K. Tanaka, T. Ichitsubo, M. Koiwa, Mater. Sci. Eng. A **312**, 118 (2001); K. Morioka, K. Tanaka, *Proceedings of the Fourth Pacific Rim International Conference on Advanced Materials and Processing* (PRICM4), edited by S. Hanada, Z. Zhong, S.W. Nam, R.N. Wright (The Japan Institute of Metals, 2001)
28. T. Mehaddene, E. Kentzinger, B. Hennion, K. Tanaka, H. Numakura, A. Marty, V. Parasote, M.C. Cadeville, M. Zemirli, V. Pierron-Bohnes, Phys. Rev. B **69**, 24304 (2004)
29. P. Barberis, Ph.D. thesis, Université Paris XI, Orsay (1992)
30. K.D. Rouse, M.J. Cooper, Acta Cryst., A **26**, 682 (1969)
31. I.A. Blech, B.L. Averbach, Phys. Rev. B **137**, 1113 (1965)
32. V. Pierron-Bohnes, C. Leroux, J.P. Ambroise, A. Menelle, J.P. Bastie, Phys. Stat. Sol. (a) **116**, 529 (1989)
33. F. Ducastelle, F. Gautier, J. Phys. F **6**, 2039 (1976)
34. A. Bieber, F. Gautier, G. Treglia, F. Ducastelle, Solid St. Comm. **39**, 149 (1981)
35. A. Bieber, F. Gautier, J. Phys. Jpn **53**, 2061 (1984)
36. A. Finel, Ph.D. thesis, Université Paris VI (1987)
37. A. Finel, in *Statistics and dynamics of Alloy Phase Transformation*, edited by P.E.A Turchi, A. Gonis, Vol. 319 of NATO Advanced Study Institute, Series B: Physics (Plenum Press, New York, 1994), p. 495
38. T. Kodera, Master thesis, Graduate School of Engineering, Hokkaido University (2004); K. Osaka, T. Kodera, H. Numakura, Y. Nose, T. Takama, *134th Meeting of the Japan Institute of Metals*, Tokyo (2004)
39. K. Yaldram, V. Pierron-Bohnes, M.C. Cadeville, M.A. Khan, J. Mater. Res. **10**, 1 (1995)
40. E. Kentzinger, M. Zemirli, V. Pierron-Bohnes, M.C. Cadeville, H. Bouzar, M. Benakki, M.A. Khan, Mater. Sc. and Eng. A **239-240**, 784 (1997)
41. P. Oramus, R. Kozubski, V. Pierron-Bohnes, M.C. Cadeville, W. Pfeiler, Phys. Rev. B **63**, 174109 (2001)
42. T. Mehaddene, O. Adjaoud, R. Kozubski, K. Tanaka, H. Numakura, J.M. Sanchez, Ch. Issro, W. Pfeiler, V. Pierron-Bohnes, submitted to Scripta Materialia
43. Ying Chen, Takaharu Atago, Tetsuo Mohri, J. Phys.: Condens. Matter **14**, 1903 (2002)